Supplemental Material for: Continuous time crystal coupled to a mechanical mode as a cavity-optomechanics-like platform

J. T. Mäkinen, 1, 2, * P. J. Heikkinen, 1, 3 S. Autti, 1, 4 V. V. Zavjalov, 1, 4 and V. B. Eltsov 1

¹Low Temperature Laboratory, Department of Applied Physics, Aalto University, FI-00076 Aalto, Finland ²QTF Centre of Excellence, Department of Applied Physics, Aalto University, FI-00076 Aalto, Finland ³Department of Physics, Royal Holloway, University of London, Egham, Surrey, TW20 0EX, UK ⁴Department of Physics, Lancaster University, Lancaster, LA1 4YB, UK (Dated: September 2, 2025)

SUPPLEMENTAL INFORMATION

Optomechanical coupling

The optomechanical coupling term g describes how the textural (order parameter) part of the trapping potential for magnons, Eq. (M17) in Methods, changes shape as the free surface of the superfluid is moving. Below we explain the different contributions to the textural free energy that compete and in combination create this effect. This allows for qualitative understanding of the coupling mechanisms. A quantitative description using a three-dimensional numerical simulation of the system is beyond the scope of the present Article.

In the superfluid B phase studied here, the superfluid state is described by an order parameter $\mathcal{A}_{\alpha i} = \Delta e^{-i\phi} R_{\alpha i}$, where Δ is the superfluid gap, superflow arises as the gradient of the phase ϕ , and $R_{\alpha i}$ is a three-dimensional rotation matrix that can be parametrised as $R_{\alpha i}(\hat{\mathbf{n}}, \theta)$. Here the rotation angle is fixed to $\theta \approx 104^{\circ}$ and the rotation axis $\hat{\mathbf{n}}$ is a unit vector field in space. The spatial variation of the order parameter relevant to the present work is entirely contained in $\hat{\mathbf{n}}$. The spatial distribution of $\hat{\mathbf{n}}$ results from the minimisation of the free energy of the order parameter configuration. Below we use the notation of Ref. 1 for these contributions.

Bulk time crystal

The leading order free energy terms governing the texture in bulk fluid are the dipole-field term

$$F_{\rm DH} = -a \int d^3r \left(\hat{\mathbf{n}} \cdot \mathbf{H}\right)^2 \,, \tag{1}$$

the dipole-velocity term

$$F_{\rm DV} = -\lambda_{\rm DV} \int d^3r \left[\hat{\mathbf{n}} \cdot (\mathbf{v}_{\rm s} - \mathbf{v}_{\rm n}) \right]^2 , \qquad (2)$$

the field-velocity term

$$F_{\rm HV} = -\lambda_{\rm HV} H^2 \int d^3r \left[\hat{\mathbf{l}} \cdot (\mathbf{v}_{\rm s} - \mathbf{v}_{\rm n}) \right]^2 , \qquad (3)$$

the first-order field-velocity term

$$F_{\rm HV1} = -\lambda_{\rm HV1} H \int d^3 r \left(\hat{\mathbf{l}} \cdot \nabla \times \mathbf{v}_{\rm n} \right) , \qquad (4)$$

and the gradient energy term

$$F_{\rm G} = \int d^3r \left[\lambda_{\rm G1} \frac{\partial R_{\alpha i}}{\partial r_i} \frac{\partial R_{\alpha j}}{\partial r_j} + \lambda_{\rm G2} \frac{\partial R_{\alpha j}}{\partial r_j} \frac{\partial R_{\alpha j}}{\partial r_i} \right]. \tag{5}$$

The definitions and theoretical evaluation of the positive-valued pressure- and temperature-dependent parameters a, $\lambda_{\rm DV}$, $\lambda_{\rm HV}$, $\lambda_{\rm HV}$, $\lambda_{\rm GI}$, and $\lambda_{\rm G2}$ can be found in Ref. 1. The vector fields that appear above are the magnetic field $H = |\mathbf{H}|$, the superfluid and normal fluid flow fields $\mathbf{v}_{\rm s}$ and $\mathbf{v}_{\rm n}$, and the orbital anisotropy axis of the Cooper pairs $\hat{\mathbf{l}} = \frac{\mathbf{H}}{|\mathbf{H}|} \cdot R_{\alpha i}(\hat{\mathbf{n}}, \theta)$. Note that the trapping potential in Eq. (M17) in Methods is given in terms of the tipping angle of the $\hat{\mathbf{l}}$ field, measured from the magnetic field direction.

In our typical experimental conditions ($T \approx 0.15T_c$, $H \gtrsim 200\,\mathrm{G}$) the dipole-velocity term (2) is always a couple of orders of magnitude smaller than the field-velocity term (3) and can be neglected. Similarly, we can neglect the first-order field-velocity term (4) since we are working with a non-rotating sample (i.e. $\nabla \times \mathbf{v}_n = 0$). Let us now estimate the magnitude of the remaining terms under these conditions.

Starting with the dipole-field term we have energy density $-F_{\rm DH}/V \sim aH^2 \approx 3 \cdot 10^{-9}\,{\rm erg/cm^3}$ when $\hat{\bf n} \parallel {\bf H}$. This assumption is satisfied near the cylinder axis, that is, where the time crystals are located in the absence of a flow field because of the cylindrical symmetry. The energy density due to the field-velocity term is $-F_{\rm HV}/V \sim \lambda_{\rm HV}H^2|v_{\rm s}|^2 \approx |v_{\rm s}|^2 \cdot 8 \cdot 10^{-8}\,{\rm erg/(cm \cdot s^2)}$ for $\hat{\bf l} \parallel {\bf v}_{\rm s}$. The terms are comparable, $F_{\rm HV} \sim F_{\rm F_{DH}}$, for realistic velocities $|v_{\rm s}| \sim 1\,{\rm mm/s}$. Finally, we can estimate the magnitude of the gradient term by noting that changes in the order parameter distribution occur typically across the magnetic healing length $\xi_{\rm H}$. Thus, $F_{\rm G} \sim (\lambda_{\rm G1} + \lambda_{\rm G2})/\xi_{\rm H}^2 \approx 10^{-9}\,{\rm erg/cm}^3$.

From the above considerations we see that the relevant terms, the dipole-field term (1), the field-velocity term (3), and the gradient energy term (5), are comparable and therefore, all relevant. We should therefore expect that the optomechanical coupling g between the moving surface and the bulk time crystal carries contributions from both static tilt of the free surface via the gradient term (5) and from the field-velocity term (3), which is absent for static tilt of the free surface.

Surface time crystal

Let us now estimate the order of magnitude of the relevant free energy terms near the free surface. The presence of a free surface gives rise to the surface-field term

$$F_{\rm SH} = -d_{\rm SH}H^2 \int d^2r \left(\hat{\mathbf{l}} \cdot \hat{\mathbf{s}}\right)^2 \,, \tag{6}$$

the first-order surface-field-velocity term

$$F_{\text{SHV1}} = -\lambda_{\text{SHV1}} H \int d^2 r \left[\hat{\mathbf{l}} \cdot \hat{\mathbf{s}} \times (\mathbf{v}_{\text{s}} - \mathbf{v}_{\text{n}}) \right], \tag{7}$$

the surface-gradient term

$$F_{\rm SG} = \lambda_{\rm SG} \int d^2 r \hat{s}_j R_{\alpha j} \frac{R_{\alpha i}}{\partial r_i} , \qquad (8)$$

and the surface-dipole term

$$F_{SD} = \int d^2r \left[b_4 \left(\hat{\mathbf{s}} \cdot \hat{\mathbf{n}} \right)^4 - b_2 \left(\hat{\mathbf{s}} \cdot \hat{\mathbf{n}} \right)^2 \right]. \tag{9}$$

Similarly to the bulk energy terms, the equations above serve as the definitions for d_{SH} , λ_{SHV1} , λ_{SG} , b_4 , and b_2 . Here $\hat{\mathbf{s}}$ is a unit vector oriented perpendicular to the surface and pointing towards the fluid.

The surface-field term (6) orients $\hat{\mathbf{l}}$ perpendicular to the surface. Its magnitude under the test conditions is $-F_{\rm SH}/A \approx 9 \cdot 10^{-9} \, {\rm erg/cm^2}$.

For velocity \mathbf{v}_s along the surface (setting $\mathbf{v}_n = 0$), such as near r = z = 0 for the flow induced by the surface wave mode we are exciting, the first-order surface-field-velocity term (7) works to orient $\hat{\mathbf{l}}$ along the surface but perpendicular to the flow. The prefactor obtains a non-zero value due to broken particle-hole symmetry and is given by¹

$$\lambda_{\text{SHV1}} = \frac{4mg_{\text{H1}}\Delta^2 \xi_{\text{GL}}^2}{h} \,, \tag{10}$$

where

$$g_{\rm H1} = \frac{1}{6} \gamma \hbar \left. \frac{\partial N}{\partial E} \right|_{E=E_{\rm F}} \ln \left(\frac{E_{\rm F}}{k_{\rm B} T_{\rm c}} \right) . \tag{11}$$

We get an estimate $\lambda_{\rm SHV1} \approx 5 \cdot 10^{-13} \, {\rm erg/(G \cdot cm^2 \cdot cm/s)}$, which results in $-F_{\rm SHV1}/A \approx 1 \cdot 10^{-10} \, {\rm erg/(cm^2 \cdot cm/s)}$. The surface-gradient term (8) acts to minimize the gradients along the surface. We can estimate its magnitude by using a similar substitution as for the bulk gradient term (5), i.e. $\partial R/\partial r \sim 1/\xi_{\rm H}$. This results in $F_{\rm SG} \sim \lambda_{\rm SG}/\xi_{\rm H} \approx 2 \cdot 10^{-10} \, {\rm erg/cm^2}$.

Finally, let us estimate the surface-dipole term. According to Ref. 1 we have $b_2(P=0) \sim 17g_D\Delta^2\xi_{\rm GL}$ and $b_2(P=0) \sim 5g_D\Delta^2\xi_{\rm GL}$, which result in a net-negative term $-F_{\rm SD}/A \sim 12g_D\Delta^2\xi_{\rm GL} \approx 1 \cdot 10^{-10}\,{\rm erg/cm^2}$.

From the above considerations we see that for realistic velocities very close to the free surface, $v_s \lesssim 1 \,\mathrm{cm/s}$, the surface-field term (6) is approximately two orders of magnitude larger than the other surface terms, suggesting that the local texture is fixed by the surface orientation and not e.g. by the first-order surface-field-velocity term (7). That is, the optomechanical coupling g for the surface time crystal should only consist of a static part that is the same regardless of whether the surface tilt is applied statically or dynamically.

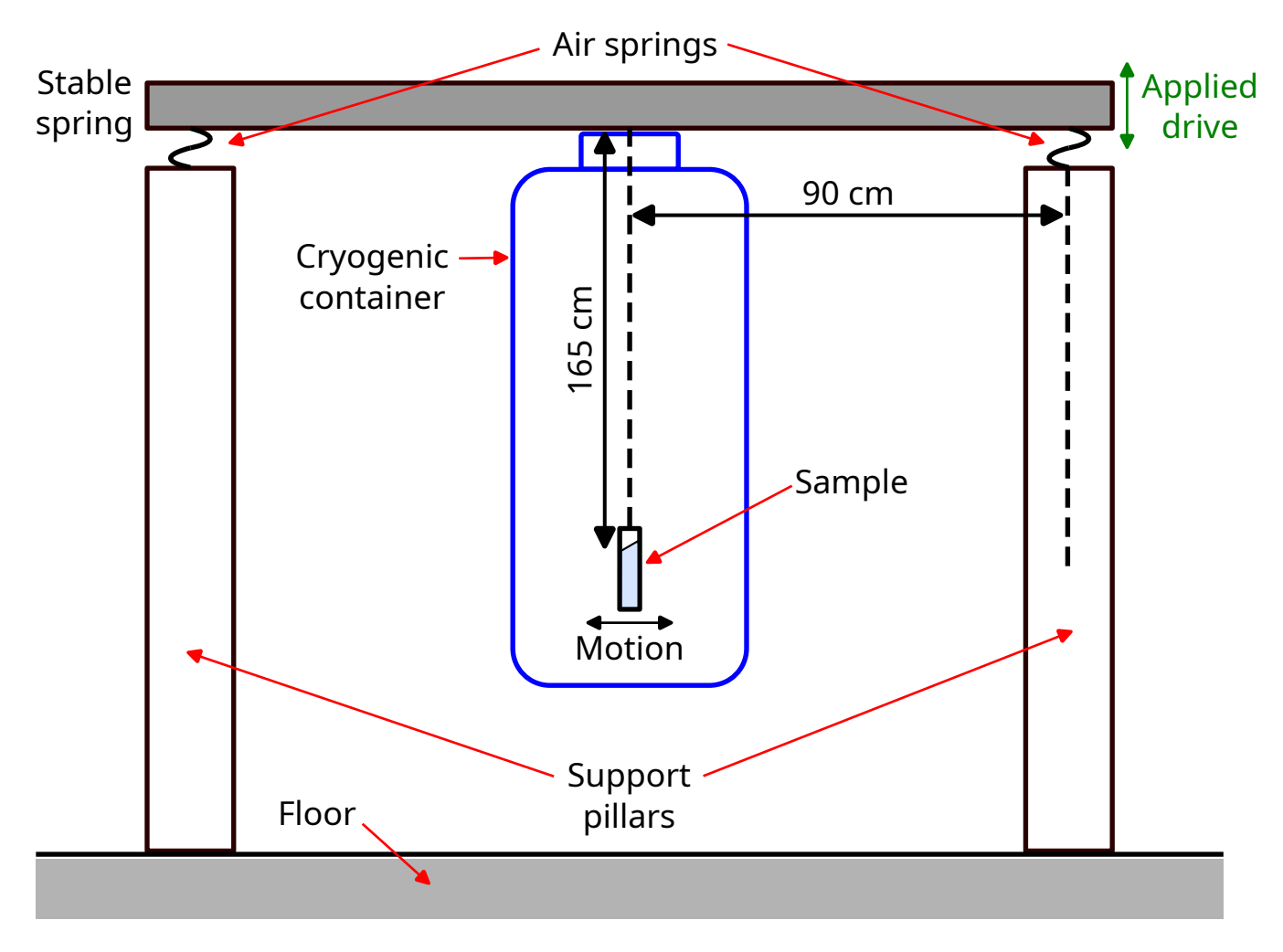
Effect of magnons

The time crystal frequency is seen changing in the experiments. This results from the magnons' contribution to the textural free energy via the spin-orbit interaction

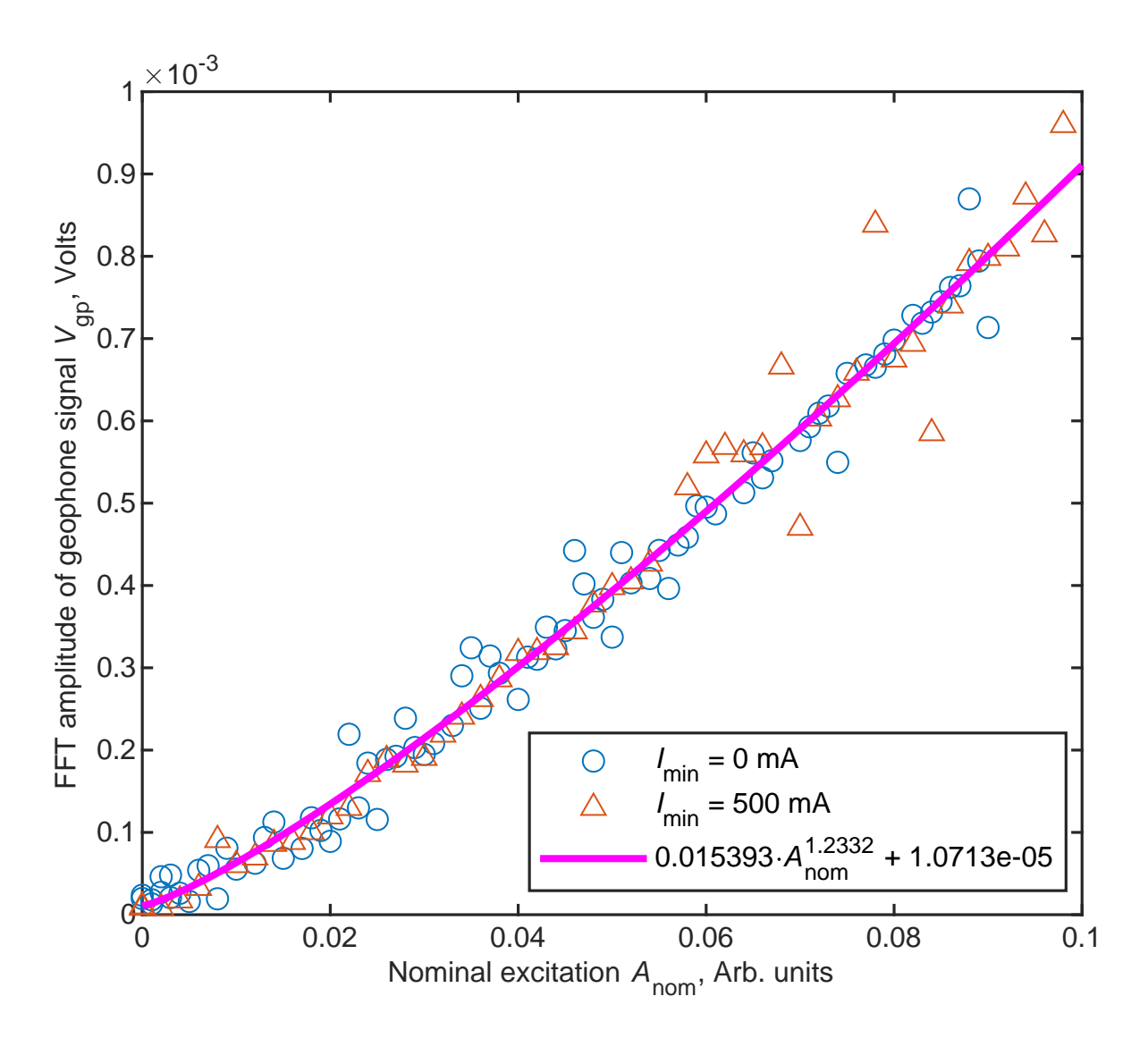
$$F_{\rm SO} = \int d^3r \left[\frac{4}{5} \hbar \frac{\Omega_{\rm L}^2}{\omega_{\rm L}} \sin^2 \left(\frac{\beta_{\rm L}}{2} \right) |\Psi|^2 \right] , \qquad (12)$$

where the wave function is related to the magnon number as $|\Psi| \sim N_{\rm m}^{1/2}$. The term (12) orients $\hat{\bf l}$ along the spin vector, i.e. along $\bf H$. Under our typical experimental conditions, $F_{\rm SO}/(V\cdot N_{\rm m})\sim 1\cdot 10^{-22}\,{\rm erg/cm^3}$. This term becomes comparable to the bulk energy terms for $N_{\rm m}\gtrsim 10^{12}$, corresponding to the end of the signal where the fitted parameter values stop changing. The time crystal phenomenology that results from this changing frequency is discussed in references 2,3, the self trapping effect resulting from Eq. (12) in references 4–6, the decay mechanisms that lead to the change in the magnon number in references 7,8, and spectral details of magnons in the trapping potential in references 9,10.

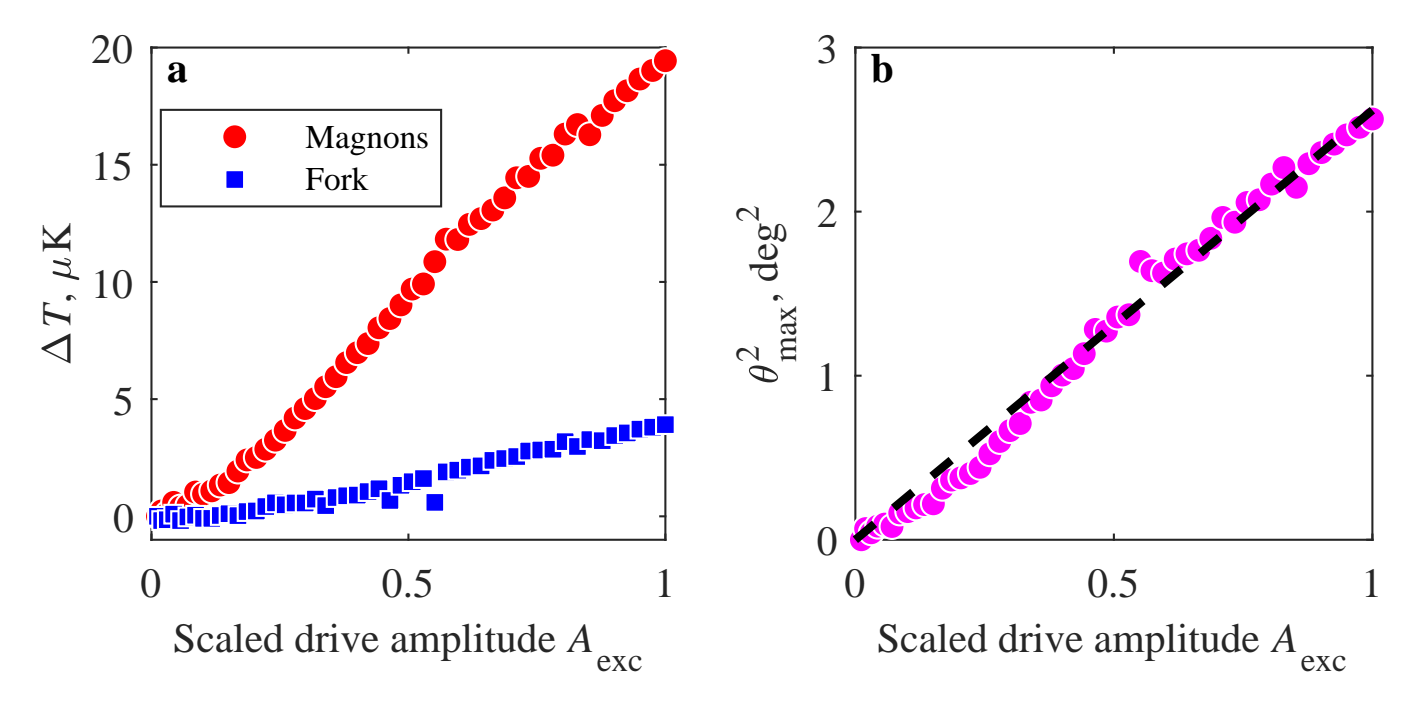
SUPPLEMENTARY FIGURES



Supplementary Figure 1. **Simplified schematic of the experimental setup.** The sample is located inside a cryogenic container centered in the middle of four support pillars at 90 cm radius. The cryogenic container is isolated against vibrations from the environment by air springs located on top of the support pillars. The liquid surface is located approximately 165 cm below the air springs. We apply periodic drive on one of the air springs to drive the sample container nearly horizontally.



Supplementary Figure 2. Calibration of the excitation amplitude To reduce noise in determination of the mechanical excitation amplitude, we estimate the functional dependence of the real excitation amplitude, measured by the geophone voltage $V_{\rm gp}$, on the nominal excitation amplitude $A_{\rm nom}$. The calibration function is displayed in the legend.



Supplementary Figure 3. **Tilt angle calibration.** a Applied surface wave excitation leads to additional heating of the sample, measured both via relaxation rate of the bulk time crystal (red points), as well as via the thermometer fork (blue points). The observed temperature between the two location separated by 14 cm is a proxy for dissipated power. **b** The measured temperature difference is converted to tilt angle using Eq. (M5) in Methods (magenta points) and fitted with a single parameter linear fit resulting in $\theta_{\rm max}^2[{\rm deg}^2] \approx 2.6182\,A_{\rm exc}$ (black dashed line).

* jere.makinen@aalto.fi

- ¹ Thuneberg, E. V. Hydrostatic theory of superfluid ³He-B. J. Low Temp. Phys. **122**, 657 (2001).
- ² Autti, S. et al. AC Josephson effect between two superfluid time crystals. Nature Materials 20, 171–174 (2021).
- ³ Autti, S. et al. Nonlinear two-level dynamics of quantum time crystals. Nature communications 13, 3090 (2022).
- ¹ Autti, S. *et al.* Self-trapping of magnon Bose-Einstein condensates in the ground state and on excited levels: From harmonic to box confinement. *Phys. Rev. Lett.* **108**, 145303 (2012).
- ⁵ Autti, S., Heikkinen, P. J., Volovik, G. E., Zavjalov, V. V. & Eltsov, V. B. Propagation of self-localized Q-ball solitons in the ³He universe. *Phys. Rev. B* **97**, 014518 (2018).
- ⁶ Autti, S., Eltsov, V. B. & Volovik, G. E. Bose analogs of the MIT bag model of hadrons in coherent precession. *JETP Lett.* **95**, 544 (2012).
- ⁷ Heikkinen, P. J. et al. Relaxation of Bose-Einstein condensates of magnons in magneto-textural traps in superfluid ³He-B. J. Low Temp. Phys. 175, 3 (2014).
- ⁸ Heikkinen, P. J., Autti, S., Eltsov, V. B., Haley, R. P. & Zavjalov, V. V. Microkelvin thermometry with Bose-Einstein condensates of magnons and applications to studies of the AB interface in superfluid ³He. J. Low Temp. Phys. 175, 681 (2014).
- ⁹ Zavjalov, V., Autti, S., Eltsov, V. B. & Heikkinen, P. Measurements of the anisotropic mass of magnons confined in a harmonic trap in superfluid ³He-B. *JETP letters* **101**, 802–807 (2015).
- Mäkinen, J. T., Autti, S. & Eltsov, V. B. Magnon Bose-Einstein condensates: From time crystals and quantum chromodynamics to vortex sensing and cosmology. *Applied Physics Letters* 124, 100502 (2024). URL https://doi.org/10.1063/5.0189649.